European **J**ournal of **Chem**istry

Check for updates

Computational insights into the corrosion inhibition potential of some pyridine derivatives: A DFT approach

Abhinay Thakur [ID] 1 and Ashish Kumar [ID] 2,*

1 *Department of Chemistry, School of Chemical Engineering and Physical Sciences, Lovely Professional University, Phagwara, 144411, India*
2 *Nalanda College of Engineering, Bihar Engineering University, Department of Science and Technology, Government of Bihar, 803108, India*

* *Corresponding author at: Department of Science and Technology, Nalanda College of Engineering, Bihar Engineering University, Government of Bihar, 803108, India.*
 e-mail: drashishchemlpu@gmail.com (A. Kumar).

RESEARCH ARTICLE

ABSTRACT

In the present investigation, the corrosion inhibition potency of five pyridine derivatives was computationally simulated and investigated by utilizing the Density Functional Theory (DFT) technique using a basis set of B3LYP/6-31++G (d,p). The predicted corrosion inhibition capacity was shown to improve in the order of 6-(trifluoromethyl) nicotinic acid > 4-(trifluoromethyl) nicotinic acid > *N*-methyl-4-chloropyridine-2-carboxamide > 2-chloro-6-trifluoromethylnicotinic acid > methyl 2-aminopyridine-4-carboxylate. Anticorrosion potentials were predicted using quantum chemical variables such as energy gap (ΔE) *i.e.* HOMO-LUMO, ionization potential (*I*), electron affinity (*A*), proportion of electrons transmitted (ΔN), hardness (η), softness (σ) and electronegativity (χ) of chemical species. It was often observed that the corrosion inhibiting rate improved with enhancement of E_{HOMO}, σ, and reduced E_{LUMO}, ΔE and η. Additionally, the electrostatic potential (ESP) mapping revealed that the heteroatoms, including the oxygen and nitrogen atoms, were the regions of anticipated electrophilic attack. This meant that atoms of oxygen and nitrogen could form bonds between the metallic substrate atoms and the investigated inhibitors. With the findings obtained, 4-methyl-2-aminopyridine-4-carboxylate showed the highest E_{HOMO} (-0.23167 eV), softness (12.40694 eV^{-1}) and the lowest E_{LUMO} (-0.7047 eV), energy gap (0.1612 eV) and hardness (0.15107 eV), therefore revealed the excellent corrosion inhibiting attribution for several crucial metals and alloys, including aluminum, mild steel, stainless steel, zinc, brass, copper, *etc.*

1. Introduction

The term 'corrosion' refers to the deterioration of metals and alloys caused by chemical/electrochemical contact with their surroundings [1-3]. The composition of the metal and the characteristics of the corroding surroundings are two major elements that affect the degree of metal corrosion. The integrity of the metal, the nature of the surface film, the physical state of the metal, and the position of the metal in the galvanic series are all included in the essence of the metal. Metals in the active site of the galvanic series corrode more rapidly than those of the noble region [4-9]. The essence of the corroding surroundings has been determined correspondingly by moisture (elevated frequency of corrosion), temperature (which is directly related to the corrosion rate), pH value, and the essence of the electrolyte (the existence of salts in the electrolyte accelerates the corrosion rate). Additionally, some industrial processes, such as acidic cleaning of boilers, acid pickling, descaling, etc., accelerate metallic corrosion [10-12]. The devasting consequences are immense and involve: risks to individuals owing to architectural collapse (*e.g.*, flyovers, automobiles, aeroplanes, *etc.*); valuation amortization of metals owing to degradation of appearance; perforation of pipelines and vessels enabling evacuation of their inclusion and potential environmental

pollution; structural stress, *etc.*; or obstruction of pipelines by sturdy corrosive materials. Numerous strategies have been used to reduce or prevent corrosion to some extent [13,14]. Among the various ways to prevent metals against corrosion is by employing inhibitors, and currently, numerous researchers are focusing their studies on the use of corrosion inhibitors, as they are widely accessible, have minimal price, are less toxic, and offer significant corrosion inhibition efficacy. In an effort to slow down the deterioration of precious metals, such molecules are segregated from the system and introduced to the abrasive environment. In particular, organic molecules with hetero-atoms like nitrogen, sulphur, and oxygen in their compositions, in addition to aromatic rings, operate as effective corrosion inhibitors. The use of such molecules over the metallic-media interface allows the inhibitors to engage with the metallic substrate by adsorption across the *p* orbitals, donating atoms, electron density, and electronic configuration of the inhibitor, thus preventing metal degradation by displacing water molecules away from the metallic substrate and forming a defensive layer over the metallic substrate by shielding the metal against further corrosive ion attacks [4,5,7,9,15-23]. Physical (electrostatic) and chemical (chemisorption) adsorption could be used to assess this adsorption. Intense electronic bonds are formed by a chemical interaction between

the metallic substrate and the inhibitor molecules during the chemisorption process. On the contrary, electrostatic couplings are prominently generated by the van der Waals force [24-30]. The type and amount of metallic charge, the electrolytes, the electronic configuration of the inhibitory molecules, the temperature of the media, the subjection period, the type of substituents, *etc.* all affect the inhibitors' ability to adsorb on the metallic surface [31-35].

Pyridine and its derivatives have demonstrated excellent inhibitory efficacy in numerous acidic and corrosive media, offering a crucial role in several disciplines, including the corrosion sciences. The six-member heteroaromatic molecule pyridine has the chemical formula C_5H_5N and is nitrogen-based. Compared to pyridine derivatives with no substitution or containing electron-withdrawing substituents, substituted pyridine derivatives having electron-donating substituents enable robust interaction with metal surfaces and function as excellent corrosion inhibitors. However, when contrasted with unsubstituted pyridine derivatives substituted at other sites, pyridine derivatives bearing either electron-withdrawing or donating substituents at the sixth or second locations exhibit comparatively significant inhibitory efficacy by developing a robust resilient chelating complex [36-39]. Many studies have recently focused on understanding the interaction involving inhibitor compounds and metallic substrates using quantum chemical methods [6,8,40-46]. To correlate the inhibitors' molecular characteristics to their effectiveness as inhibitors, a number of quantum chemical techniques have been devised. The hypothesis of functionality of conceptual density such as DFT analysis, although, is arguably the most liked and optimist theory in use today [37,39,47-51]. A computational modelling technique called density functional theory (DFT) is frequently utilised to explore the innate characteristics of molecules. For inhibitors, research is focused mainly on predicting chemical quality, including energy gap, HOMO-LUMO, chemical hardness and softness, ionization potential, electronegativity, and electron affinity of chemical species [52-54].

Tang *et al.* [39] used the DFT strategy to examine the effects of different molar proportions of pyridine derivatives (4-methylpyridine *i.e.*, 4-MP and 4-PQ) and sulfur including compounds (4-methylpyridine and its quaternary ammonium salts *i.e.* TU and TZ) for the ability of carbon steel to resist corrosion in a CO_2-saturated 3.5 weight percent NaCl media. While sulphur-containing molecules having lower volumes fill in voids, pyridine derivative molecules having higher volumes bind first on the metallic substrate. Figure 1 shows the density profiles of FMOs of 4-MP and 4-PQ, as well as TU and TZ. The heterocyclic ring comprising the sulphur and nitrogen atoms is where the forefront orbit dispersion is primarily focused. The chemical potential is related to quantum characteristics such as electronegativity (χ), in which a higher value indicates a stronger inhibition effectiveness. While, the greater polarizability and improved inhibitory efficacy are implied by the lower chemical hardness (η). The ΔE is the most important variable, and a drop in ΔE results in an elevation in the action of reactivity. Softness is the inverse of η; therefore, a higher value is associated with increased effectiveness. The lowest *E* for the four inhibitors was for TU and the highest *E* for the mixture of TU and 4-PQ was for 4-PQ. It matches the results of the investigation itself. While sulphur-containing compounds and 4-PQ were combined in the right mole proportion, a thick adsorption layer was created.

Similarly, Saddy *et al.* [38] evaluated the inhibition effect of 6-bromo-2-(4-chlorophenyl)-3-pyridine derivatives of imidazole[4, 5-b](prop-2-yn-1-yl)6-bromo-2-(3*H*)-imidazol[4, 5-b] pyridine (SB9a) and (4-chlorophenyl)-3-decyl-3*H*-imidazo [4,5-b]pyridine (SB14a) for mild steel (MS) corrosion in 1 M HCl. The DFT approach at the B3LYP level using the 6-31G(d,p) basis set was utilized to optimize molecular configurations and

find specific geometric variables. The dihedral angles and bond lengths confirmed the optimum structural layouts of the two examined variants. Because of their considerable polarization, bromine and chlorine molecules are likely to adhere to the MS interface more effectively. As the examined inhibitors were able to achieve a rate of 8% for SB9a and 90% for SB14a 0.1 mM, they demonstrated a significant level of inhibitory efficacy.

In this article, we provide the results of an investigation of various pyridine derivatives as corrosion inhibitors utilising the DFT technique basis set of DFT/B3LYP/6-31++G (d,p). Pyridine derivatives including 2-chloro-6-trifluoromethyl nicotinic acid, 4-(trifluoromethyl) nicotinic acid, 6-(trifluoro methyl) nicotinic acid, methyl 2-aminopyridine-4-carboxylate and *N*-methyl-4-chloropyridine-2-carboxamide, meet all the criteria for the effectiveness of a significant corrosion inhibitor according to the literature [36-39,55-58].

2. Calculation methodology

The behavior of corrosion inhibitors in various abrasive solutions and on the metallic substrate is gradually being explained by computational software, which is emerging as a widely used and trustworthy technique [59,60]. A computational modelling technique called density functional theory (DFT) is frequently used to explore the innate characteristics of molecules. For inhibitors, research is primarily focused on predicting chemical characteristics of chemical species, including the highest occupied molecular orbital–lowest unoccupied molecular orbital (HOMO–LUMO), electron affinity (A), ionization potential (I), energy gap (ΔE), hardness (η), the fraction of electrons transferred (ΔN), softness (σ) and electronegativity (χ) of chemical species.

The effectiveness of the five specified pyridine derivatives was predicted using theoretical analyses in the following work: Initially, the structural characteristics of the pyridine derivatives including 2-chloro-6-trifluoromethylnicotinic acid, 4-(trifluoromethyl) nicotinic acid, 6-(trifluoromethyl) nicotinic acid, methyl 2-aminopyridine-4-carboxylate and *N*-methyl-4-chloropyridine-2-carboxamide were investigated (Table 1). All compounds were geometrically optimized using the DFT / B3LYP approach linked to 6-31G++(d,p) basis sets, which is frequently used in the analysis of organic corrosion inhibitors (CI) using the Gaussian 03W programming suite. Then, numerous pertinent global and local variables of the electronic configuration of the molecule were calculated. In addition to the lowest unoccupied molecular orbital (E_{LUMO}) and the highest occupied molecular orbital (E_{HOMO}), as well as the ionization potential (*I*, Equation (1)), electron affinity (*A*, Equation (2)), energy gap (ΔE, Equation (3)), the fraction of electrons transferred (ΔN, Equation (4)), hardness (η, Equation (5)), softness (σ, Equation (6)) and electronegativity (χ, Equation (7)) are included. Furthermore, the FMOs of each pyridine derivative's FMOs (HOMO and LUMO) repartitions and 2D electrostatic potential maps were calculated.

The Equation (1) relates an inhibiting molecule's ionization potential (*I*), which is correlated with the E_{HOMO}, to its capability to donate electrons into the minimally positioned vacant orbitals of a metal:

$$I = -E_{HOMO} \tag{1}$$

Additionally, as stated in Equation (2), an inhibitor's electron affinity (*A*), which relates to the E_{LUMO} and denotes the propensity of the inhibitor to receive electrons:

$$A = -E_{LUMO} \tag{2}$$

The predicted corrosion inhibition ability improves when the ΔE of inhibitors narrows due to a commensurate rise in their reactivity. The term relates this band gap to *I* and *A*, as shown in Equation (3):

HOMO   **LUMO**

4-Methylpyridine (4-MP)

4-Quaternary ammonium salts (4-PQ)
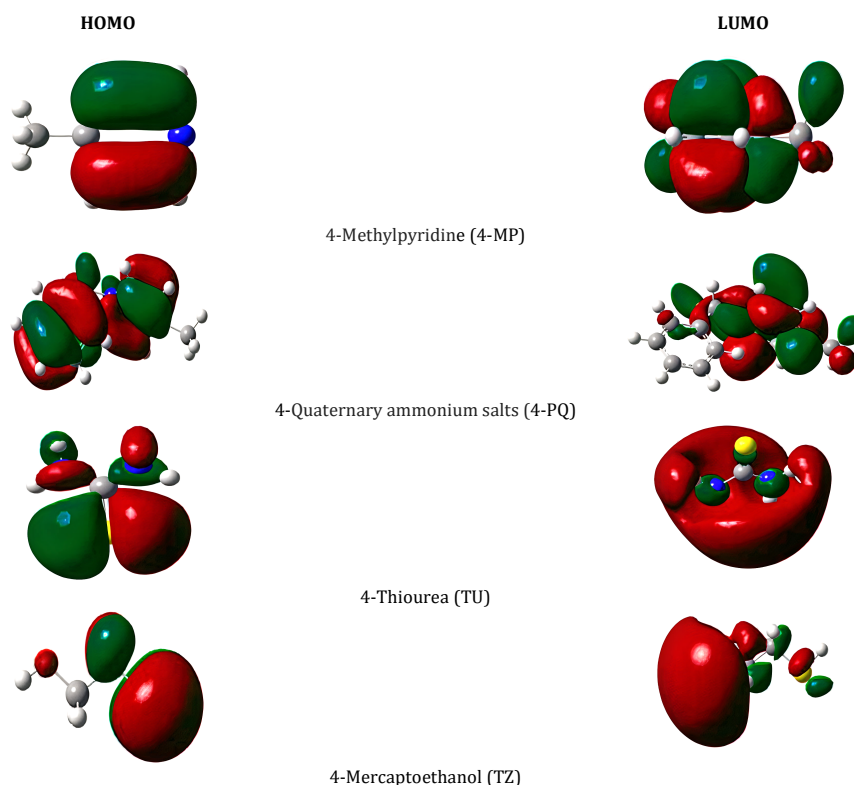
4-Thiourea (TU)

4-Mercaptoethanol (TZ)

Figure 1. Illustration of the FMOs, *i.e.*, HOMO and LUMO of pyridine derivatives and sulphur-containing compounds. Adapted with permission from [39].

$$\Delta E = I - A \tag{3}$$

The global hardness (η) is another variable connected to *I* and *A*, as indicated in Equation (5). This metric, which measures the resistance of a system to releasing electrons, is used to forecast the reactivity of a molecule. According to Equation (4), Δ*N* (amount of electrons transit) is the second derivative of Δ*E* with regard to Δ*N*:

$$\Delta N = \frac{\phi_{Fe} - \chi_{inh}}{2(\eta_{Fe} + \eta_{inh})} \tag{4}$$

$$\eta = \left(\frac{I - A}{2}\right) \tag{5}$$

Global softness (σ) is an additional indicator of chemical reactivity and the inverse of global softness in half, as noticed in Equation (6):

$$\sigma = 1 / \eta \tag{6}$$

The variable utilized to compute Δ*N* is electronegativity (χ), which describes the orientation of electron transport across an inhibitor and metal until a similar chemical potential is reached between the two (number of transferred electrons). According to the expression, the E_{HOMO} and E_{LUMO} *of a molecule* are connected to *I* and *A* as stated in Equation (7):
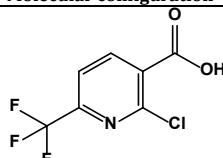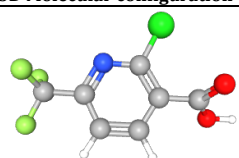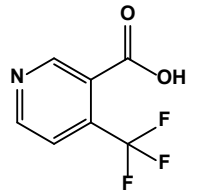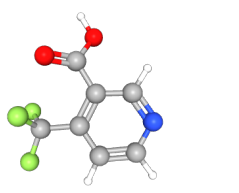
$$\chi = \left(\frac{I + A}{2}\right) \tag{7}$$
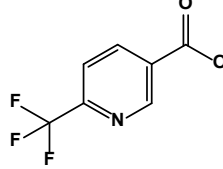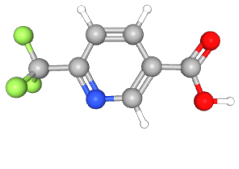
3. Results and discussion

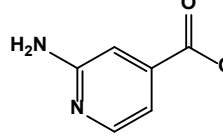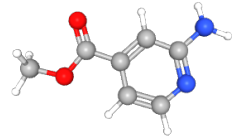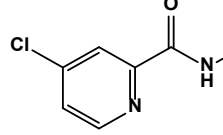Using the Gaussian 09 tool, the quantum chemistry computations were carried out. The computations are predicated on the DFT methodology, another technique for describing the basic state of molecular systems. Its effectiveness could be attributed to the fact that it applies to a wide range of systems (organic molecules, materials, complexes, *etc.*) and that its computing period is considerably shorter than that of post-Hartree-Fock approaches. It is commonly employed to characterize interactions amongst metal inhibitors. DFT analyses for molecules have been performed and optimized utilizing the hybrid functional B3LYP. Numerous observations have been provided in this subsection, including electrostatic potential maps (ESP), total density, surface contours, and HOMO and LUMO findings. The configuration of the HOMO and LUMO orbitals is considered crucial to determining a molecule's reactivity and the evolution of chemical reactions. It is feasible to observe the electron dispersion and, consequently, locate the centers or regions of electron density in each molecule by employing ESP mapping.

The contour mappings of electron density show that heteroatoms on the investigated molecular inhibitors, including oxygen and nitrogen atoms, present favorable interaction locations when considering the distinction between the roles of the heteroatoms and the other atom. Bonding contacts across inhibitor substrates and metallic surfaces are formed by interaction regions enclosed by a dark red border. As per the contour depiction of electrostatic by using the DFT/B3LYP/6-31++G(d,p) basis set, the dark red color is specifically surrounded by electronegative molecules and their areas in pyridine derivative molecules, while the green color is dispersed in the positive potential area. In contrast to the Δ*N*, which is regarded as the most important variable because it incorporates multiple earlier variables, the electronegativity (χ) and global hardness (η) parameters are crucial to thoroughly describing the reactivity of an inhibitor. A high level of electrophilicity denotes a strong electrophile, whereas a low number denotes a strong nucleophile that features positive charges, the former of which often corresponds to the charges on a metal substrate. FMOs such as E_{HOMO} and E_{LUMO} are crucial indicators for predicting reactive chemical entities.

Table 1. Name, formulas, and molecular configuration of the investigated pyridine derivatives.

Name	Formula	Molecular configuration	3D Molecular configuration
2-Chloro-6-trifluoromethylnicotinic acid	C$_7$H$_3$ClF$_3$NO$_2$		
4-(Trifluoromethyl)nicotinic acid	C$_7$H$_4$F$_3$NO$_2$		
6-(Trifluoromethyl)nicotinic acid	C$_7$H$_4$F$_3$NO$_2$		
Methyl 2-aminopyridine-4-carboxylate	C$_6$H$_7$N$_3$O$_2$		
N-Methyl-4-chloropyridine-2-carboxamide	C$_7$H$_7$ClN$_2$O		

Typically, E_{HOMO} refers to a molecule's capacity to offer an electron. Therefore, if E_{HOMO} increases, it means that there is a larger propensity to contribute electrons to the suitable acceptor that possesses an unoccupied orbital. The metallic substrate may absorb protective elements more easily due to the significant value of E_{HOMO}. By accelerating the mechanism of transfer by the adsorbent sheet, the inhibitor's preventive effectiveness was improved. Both the chemisorption and physisorption processes are confirmed by the acquired quantum chemical information, according to the E_{HOMO} that has the negative value assessed and other thermodynamic proper-ties. Because the energy gap is correlated with the softness and/or hardness of the inhibitor molecules, a significant value for ΔE denotes poor reactivity of the inhibitor molecules. Although the soft molecule possesses an energy gap smaller than that of the rigid one, the soft molecule is less reactive. Figures 2-6 depict the optimized molecular geometries, frontier molecular orbitals (FMOs) (*i.e.*, HOMO and LUMO), ESP maps, surface contours, and total electronic density of the pyridine derivatives.

Through the investigation of Figures 2-6, it can be observed that HOMO and LUMO in the molecules of 2-chloro-6-trifluoro methylnicotinic acid, 6-(trifluoromethyl) nicotinic acid, 4-(trifluoromethyl) nicotinic acid, methyl 2-aminopyridine-4-carboxylate, and *N*-methyl-4-chloropyridine-2-carboxamide are located approximately throughout the molecular fractions. This finding suggests that all five molecules are involved in charge sharing. The presence of heteroatom moieties and an aromatic ring configuration in their molecular compositions, correspondingly, is related to their relatively large participation in charge. Following these considerations, it has been shown that the molecules 2-chloro-6-trifluoromethylnicotinic acid, 6-(trifluoromethyl) nicotinic acid, methyl 2-aminopyridine-4-carboxylate, 4-(trifluoromethyl) nicotinic acid and *N*-methyl-4-

chloropyridine-2-carboxamide have exceptional anticorrosive capabilities that are responsible for corrosion mitigation. Electrostatic potential surface ESP maps could offer an instinctive approach to quantifying polarity that facilitates the evaluation of the corrosion process. The negative electrostatic potential portion (red tint) is susceptible to nucleophilic attack, whereas the positive potential portion (blue tint) is susceptible to electrophilic attacks. Red areas are typically found around the heteroatom (oxygen), which could establish a covalent bond with the Fe atom, as shown in Figures 2-6. Positive potential regions are found near hydrogen and carbon atoms, which are ideal targets for electrophilic attack.

2-Chloro-6-trifluoromethylnicotinic acid, 6-(trifluoro methyl) nicotinic acid, methyl 2-aminopyridine-4-carboxylate, 4-(trifluoromethyl) nicotinic acid and *N*-methyl-4-chloro pyridine-2-carboxamide offer a superior potential to gain electrons from the metallic surface because it has a higher negative potential. Similar findings were obtained from the ΔN and the frontier molecular orbitals (E_{HOMO} and E_{LUMO}) investigations (Table 2). The acquired quantum chemical characteristics of the listed molecules are reported in Table 2. Low E_{LUMO} levels resemble the electron acceptance capacity of a molecule, while the maximum E_{HOMO} level of a molecule demonstrates its electron transmission capacity. Another statistic is the energy gap (ΔE); the difference in energy between E_{HOMO} and E_{LUMO}, which is crucial to consider when examining and explaining the resilience indices of a corrosion inhibitor.

The stronger and more reciprocal the interaction between the metallic substrate and the inhibitor, the lower ΔE value must be. In this scenario, among all, the value of ΔE of methyl 2-aminopyridine-4-carboxylate comes out to be the smallest, *i.e.*, 0.1612 eV, which could be ascribed to the availability of the hetero atom and the aromatic ring in its structure as compared
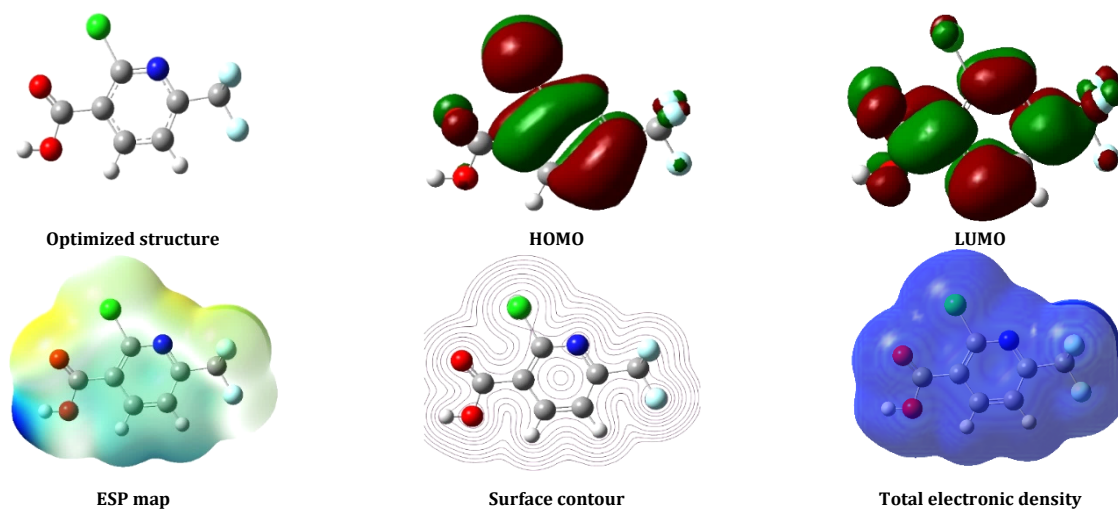
Figure 2. Optimized molecular geometries, FMOs (HOMO and LUMO), ESP maps, surface contours and total electronic density illustration of the 2-chloro-6-trifluoromethylnicotinic acid.
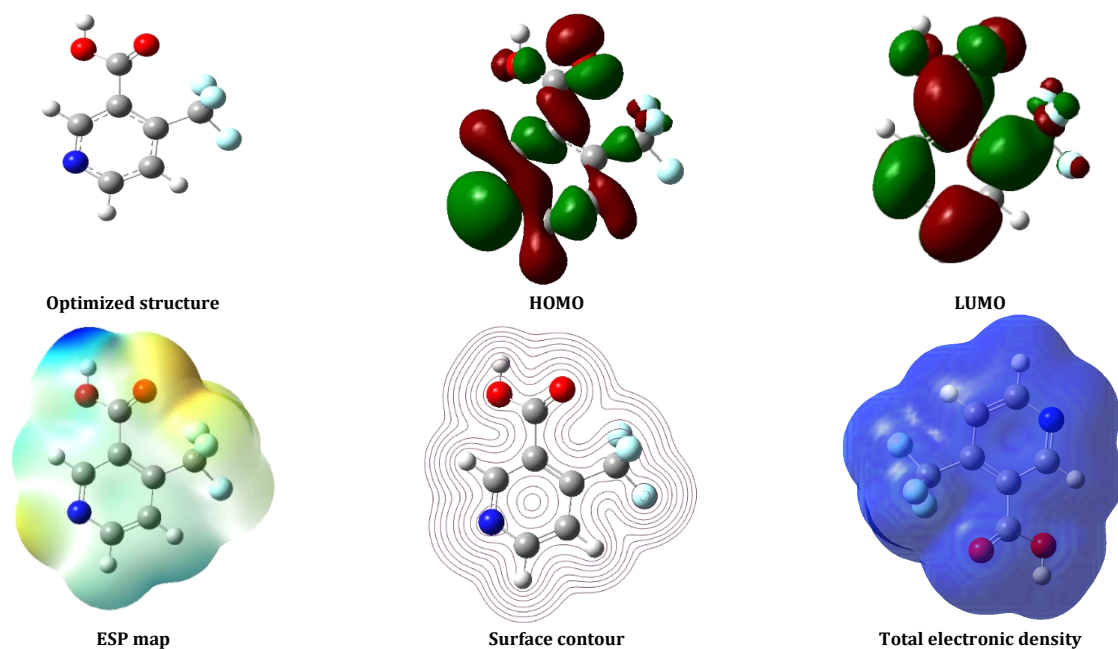

Figure 3. Optimized molecular geometries, FMOs (HOMO and LUMO), ESP maps, surface contours and total electronic density illustration of the 4-(trifluoromethyl)nicotinic acid.

Figure 4. Optimized molecular geometries, FMOs (HOMO and LUMO), ESP maps, surface contours and total electronic density illustration of the 6-(trifluoromethyl)nicotinic acid.
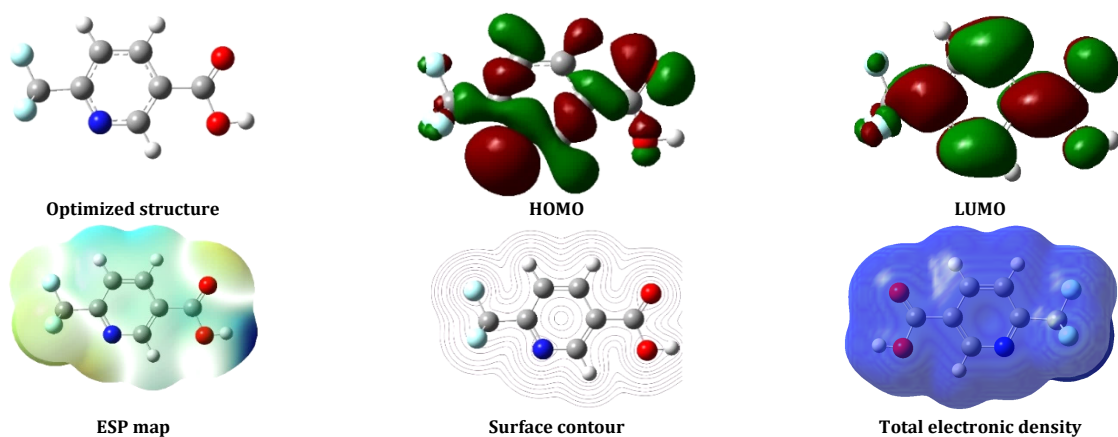
Table 2. Data findings of quantum chemical variables using the DFT/B3LYP/6-31++G(d, p) basis set.

Parameters	2-Chloro-6-trifluoro methylnicotinic acid	4-(Trifluoromethyl) nicotinic acid	6-(Trifluoromethyl) nicotinic acid	Methyl 2-amino pyridine-4-carboxylate	N-Methyl-4-chloropyridine -2-carboxamide
E_{HOMO} (eV)	-0.29708	-0.29299	-0.29951	-0.23167	-0.26578
E_{LUMO} (eV)	-0.10600	-0.09613	-0.09990	-0.07047	-0.07285
ΔE (eV)	0.19108	0.19686	0.19961	0.16120	0.19293
I (eV)	0.29708	0.29299	0.29951	0.23167	0.26578
A (eV)	0.10600	0.09613	0.09990	0.07047	0.07285
η (eV)	0.20154	0.19456	0.19970	0.15107	0.16932
χ (eV)	0.09554	0.09843	0.09981	0.08060	0.09647
σ (eV^{-1})	10.46680	10.15950	10.01953	12.40694	10.36645
ΔN_{max} (eV)	0.23256	0.23994	0.24304	0.25823	0.23637
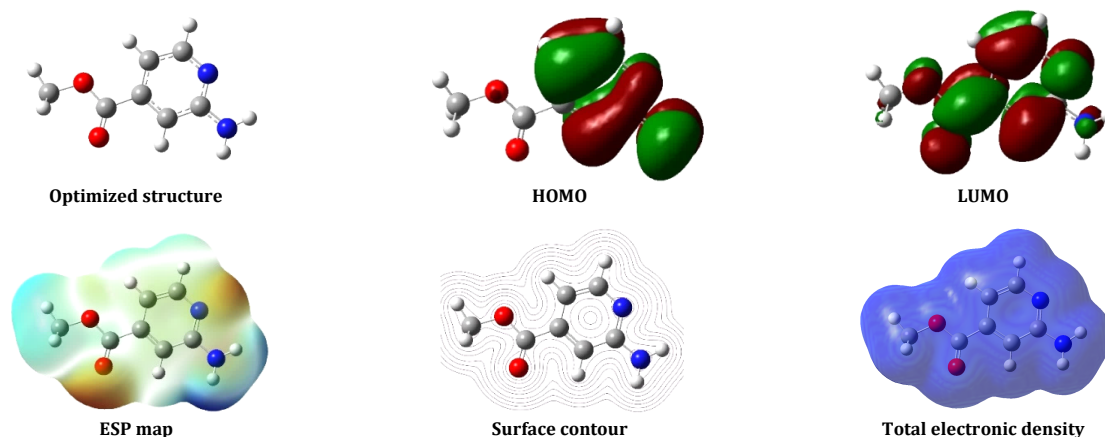
Figure 5. Optimized molecular geometries, FMOs (HOMO and LUMO), ESP maps, surface contours and total electronic density illustration of the methyl 2-aminopyridine-4-carboxylate.
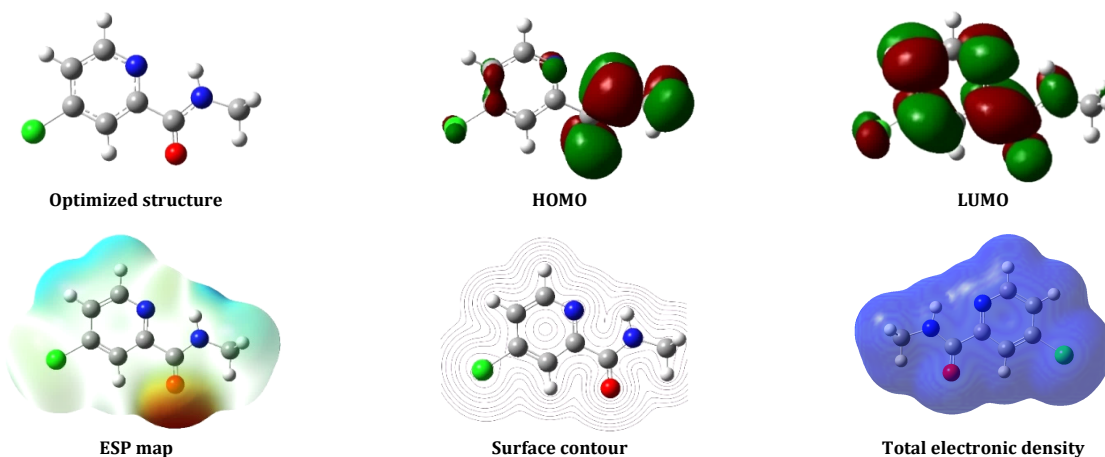
Figure 6. Optimized molecular geometries, FMOs (HOMO and LUMO), ESP maps, surface contours and total electronic density illustration of the *N*-methyl-4-chloropyridine-2-carboxamide.

to 2-chloro-6-trifluoro methylnicotinic acid, 6-(trifluoromethyl) nicotinic acid, *N*-methyl-4-chloropyridine-2-carboxamide and 4-(tri fluoromethyl) nicotinic acid.

Table 2 shows that all molecules have low E_{LUMO} and significant E_{HOMO} values. This indicates that each inhibitor molecule has a substantial capacity for attaching to metallic surfaces, which significantly reduces corrosion. It is also explained in several articles that the negative value of E_{HOMO} represents physical adsorption. In the latest study, the E_{HOMO} values of all compounds come out to be negative, therefore, depicting more chances of physical adsorption than chemical adsorption. The tendency of a molecule to transmit electrons to the vacant orbital is denoted by the character ΔN. The ΔN value is a sign of the persistence and chemical interaction of the inhibitor substances. In reality, a positive and higher value of N reveals the stronger inhibitory activity of a molecule. In this case, again the ΔN value of methyl 2-aminopyridine-4-carboxylate (0.258232 eV) came out to be the maximum after

all remaining molecules 2-chloro-6-trifluoro methylnicotinic acid, 6-(trifluoromethyl)nicotinic acid, *N*-methyl-4-chloro-pyridine-2-carboxamide and 4-(trifluoromethyl) nicotinic acid have quite positive and similar ΔN values of 0.23256, 0.243039, 0.2363722 and 0.23994 eV which corresponds to their better chemical reactivity and stability. It is also well mentioned that η with a low value proposes a higher IE%. Through Table 2, it can be observed that methyl 2-aminopyridine-4-carboxylate has a low value of η, *i.e.*, 0.15107 eV followed by 2-chloro-6-trifluoromethylnicotinic acid (0.20154 eV), 6-(trifluoromethyl) nicotinic acid (0.19970 eV), *N*-methyl-4-chloropyridine-2-carboxamide (0.169315 eV) and 4-(trifluoromethyl) nicotinic acid (0.19456 eV), again corresponds to the better inhibitor efficiency of the derivatives. Unlike the value of ΔN, the value of η is also in great agreement with the empirical findings. This shows that all investigated pyridine derivatives are the least susceptible to charge donation and acceptance. As a result, they

show that the listed pyridine derivatives can possess a strong corrosion inhibitory effect on metal surfaces.

4. Conclusion

In summary, a DFT calculation was performed with the DFT/B3LYP/6-31++G (d,p) basis set to analyse and measure the corrosion inhibition potential of five pyridine derivatives including 2-chloro-6-trifluoromethylnicotinic acid, 6-(trifluoro methyl) nicotinic acid, 4-(trifluoromethyl) nicotinic acid, methyl 2-aminopyridine-4-carboxylate and *N*-methyl-4-chloro pyridine-2-carboxamide for their possible potent corrosion inhibition potential for several metals and alloys. From the findings of the DFT analysis, it was observed that methyl-2-aminopyridine-4-carboxylate has a minimal electronegativity value compared to 2-chloro-6-trifluoromethylnicotinic acid, 4-(trifluoromethyl) nicotinic acid, 6-(trifluoromethyl) nicotinic acid and *N*-methyl-4-chloropyridine-2-carboxamide. Additionally, the value of ΔE of methyl 2-aminopyridine-4-carboxylate comes out to be the smallest, that is, 0.1612 eV, which could be ascribed to the availability of the heteroatom and aromatic ring in its structure compared to other molecules, which showed its stronger and mutual connection across the metallic surface and the inhibitor. Moreover, the ΔN value of methyl 2-aminopyridine-4-carboxylate (0.258232 eV) came out to be the maximum after all remaining molecules 2-chloro-6-trifluoromethylnicotinic acid, 6-(trifluoromethyl) nicotinic acid, 4-(trifluoromethyl) nicotinic acid and *N*-methyl-4-chloro pyridine-2-carboxamide have quite positive and similar ΔN values of 0.23256, 0.243039, 0.23994 and 0.2363722 eV, which corresponds to their better chemical reactivity and stability. Therefore, methyl 2-aminopyridine-4-carboxylate is more prone to react as an electron donor compared to other compounds, making it an effective corrosion inhibitor for a range of vital metals and alloys such as mild steel, aluminium, stainless steel, zinc, brass, copper, *etc*.

Acknowledgements

Disclosure statement DS

Conflict of interest: The authors declare that they have no conflict of interest. Ethical approval All ethical guidelines have been adhered to.

CRediT authorship contribution statement CR

Conceptualization, Me: Abhinay Thakur; Methodology: Abhinay Thakur; Software: Abhinay Thakur; Validation: Ashish Kumar and Abhinay Thakur; Formal Analysis: Abhinay Thakur; Investigation: Ashish Kumar; Data Curation: Ashish Kumar; Writing - Original Draft: Abhinay Thakur and Ashish Kumar.

ORCID iD and Email ✉

Abhinay Thakur
✉ thakurabhinay96@gmail.com
iD https://orcid.org/0000-0002-7186-1639
Ashish Kumar
✉ drashishchemlpu@gmail.com
iD https://orcid.org/0000-0002-2003-6209

References

[1].　Bawazeer, T. M.; El-Ghamry, H. A.; Farghaly, T. A.; Fawzy, A. Novel 1,3,4-thiadiazolethiosemicarbazones derivatives and their divalent cobalt-complexes: Synthesis, characterization and their efficiencies for acidic corrosion inhibition of carbon steel. *J. Inorg. Organomet. Polym. Mater.* **2020**, *30*, 1609–1620.

[2].　Li, P.; School of Materials Engineering, Shanghai University of Engineering Science, Shanghai 201620, China Corrosion inhibition effect of N-(4-diethylaminobenzyl) Quaternary ammonium chitosan

[3].　for X80 pipeline steel in hydrochloric acid solution. *Int. J. Electrochem. Sci.* **2021**, 150931.

[3].　Cui, M.; Key Laboratory of Impact and Safety Engineering, Ministry of Education, School of Mechanical Engineering and Mechanics, Ningbo University, Ningbo, 315211, China Microwave synthesis of Eco-friendly nitrogen doped carbon dots for the corrosion inhibition of Q235 carbon steel in 0.1 M HCl. *Int. J. Electrochem. Sci.* **2021**, 151019.

[4].　Bashir, S.; Thakur, A.; Lgaz, H.; Chung, I.-M.; Kumar, A. Corrosion inhibition efficiency of bronopol on aluminium in 0.5 M HCl solution: Insights from experimental and quantum chemical studies. *Surf. Interfaces* **2020**, *20*, 100542.

[5].　Thakur, A.; Sharma, S.; Ganjoo, R.; Assad, H.; Kumar, A. Anti-corrosive potential of the sustainable corrosion inhibitors based on biomass waste: A review on preceding and perspective research. *J. Phys. Conf. Ser.* **2022**, *2267*, 012079.

[6].　Thakur, A.; Kumar, A.; Sharma, S.; Ganjoo, R.; Assad, H. Computational and experimental studies on the efficiency of Sonchus arvensis as green corrosion inhibitor for mild steel in 0.5 M HCl solution. *Mater. Today* **2022**, *66*, 609–621.

[7].　Bashir, S.; Thakur, A.; Lgaz, H.; Chung, I.-M.; Kumar, A. Corrosion inhibition performance of acarbose on mild steel corrosion in acidic medium: An experimental and computational study. *Arab. J. Sci. Eng.* **2020**, *45*, 4773–4783.

[8].　Thakur, A.; Kumar, A.; Kaya, S.; Marzouki, R.; Zhang, F.; Guo, L. Recent advancements in surface modification, characterization and functionalization for enhancing the biocompatibility and corrosion resistance of biomedical implants. *Coatings* **2022**, *12*, 1459.

[9].　Bashir, S.; Thakur, A.; Lgaz, H.; Chung, I.-M.; Kumar, A. Computational and experimental studies on Phenylephrine as anti-corrosion substance of mild steel in acidic medium. *J. Mol. Liq.* **2019**, *293*, 111539.

[10].　Razizadeh, M.; Mahdavian, M.; Ramezanzadeh, B.; Alibakhshi, E.; Jamali, S. Synthesis of hybrid organic–inorganic inhibitive pigment based on basil extract and zinc cation for application in protective construction coatings. *Constr. Build. Mater.* **2021**, *287*, 123034.

[11].　Jimoh, I.; Usman, B. Corrosion Inhibition Potential of Ethanol Extract of Acacia nilotica Leaves on Mild Steel in an Acidic Medium. *Port. Electrochim. Acta* **2021**, *39*, 105–128.

[12].　Fouda, A. E. S.; Motaal, S. M. A.; Ahmed, A. S.; Sallam, H. B. Corrosion protection of carbon steel in 2M HCl using Aizoon canariense extract. *Biointerface Res. Appl. Chem.* **2021**, *12*, 230–243.

[13].　Bashir, S.; Sharma, V.; Dhaundiyal, P.; Shafi, N.; Kumar, A. Gymneme Sylvestre as a green corrosion inhibitor for aluminum in an acidic medium. *Port. Electrochim. Acta* **2021**, *39*, 199–212.

[14].　Zadeh, F. M. H.; Khaleghi, M.; Bordbar, S.; Jafari, A. Myrtus communis extract: a bio-controller for microbial corrosion induced by sulphate reducing bacteria. *Corros. Eng. Sci. Technol.* **2021**, *56*, 269–278.

[15].　Sharma, S.; Ganjoo, R.; Kr. Saha, S.; Kang, N.; Thakur, A.; Assad, H.; Sharma, V.; Kumar, A. Experimental and theoretical analysis of baclofen as a potential corrosion inhibitor for mild steel surface in HCl medium. *J. Adhes. Sci. Technol.* **2021**, 1–26.

[16].　Thakur, A.; Kumar, A.; Kaya, S.; Vo, D.-V. N.; Sharma, A. Suppressing inhibitory compounds by nanomaterials for highly efficient biofuel production: A review. *Fuel (Lond.)* **2022**, *312*, 122934.

[17].　Sharma, S.; Ganjoo, R.; Kr. Saha, S.; Kang, N.; Thakur, A.; Assad, H.; Kumar, A. Investigation of inhibitive performance of Betahistine dihydrochloride on mild steel in 1 M HCl solution. *J. Mol. Liq.* **2022**, *347*, 118383.

[18].　Kumar, A.; Thakur, A. Encapsulated nanoparticles in organic polymers for corrosion inhibition. In *Corrosion Protection at the Nanoscale*; Elsevier, 2020; pp. 345–362.

[19].　Ganjoo, R.; Sharma, S.; Thakur, A.; Kumar, A. Thermodynamic study of corrosion inhibition of Dioctylsulfosuccinate Sodium Salt as corrosion inhibitor against mild steel in 1 M HCl. *Mater. Today* **2022**, *66*, 529–533.

[20].　Ganjoo, R.; Bharmal, A.; Sharma, S.; Thakur, A.; Assad, H.; Kumar, A. Imidazolium based ionic liquids as green corrosion inhibitors against corrosion of mild steel in acidic media. *J. Phys. Conf. Ser.* **2022**, *2267*, 012023.

[21].　Thakur, A.; Kaya, S.; Abousalem, A. S.; Kumar, A. Experimental, DFT and MC simulation analysis of Vicia Sativa weed aerial extract as sustainable and eco-benign corrosion inhibitor for mild steel in acidic environment. *Sustain. Chem. Pharm.* **2022**, *29*, 100785.

[22].　Thakur, A.; Kumar, A. Recent advances on rapid detection and remediation of environmental pollutants utilizing nanomaterials-based (bio)sensors. *Sci. Total Environ.* **2022**, *834*, 155219.

[23].　Sharma, S.; Ganjoo, R.; Thakur, A.; Kumar, A. Investigation of corrosion performance of expired Irnocam on the mild steel in acidic medium. *Mater. Today* **2022**, *66*, 540–543.

[24].　Al-Turkustani, A. M. Thermodynamic, chemical and electrochemical investigation of pandanus tectorius extract as corrosion inhibitor for steel in sulfuric acid solutions. *Eur. J. Chem.* **2013**, *4*, 303–310.

[25].　Assad, H.; Thakur, A.; Bharmal, A.; Sharma, S.; Ganjoo, R.; Kaya, S. 2 Corrosion inhibitors: fundamental concepts and selection metrics. In *Corrosion Mitigation*; De Gruyter, 2022; pp. 19–50.

[26]. Burkhanova, T. M.; Krysantieva, A. I.; Babashkina, M. G.; Konyaeva, I. A.; Monina, L. N.; Goncharenko, A. N.; Safin, D. A. In silico analyses of betulin: DFT studies, corrosion inhibition properties, ADMET prediction, and molecular docking with a series of SARS-CoV-2 and monkeypox proteins. *Struc. Chem.* **2022**, *1*, 1-12.

[27]. Ress, J.; Martin, U.; Breimaier, K.; Bastidas, D. M. Electrochemical and DFT Study of NaNO2/NaNO3 Corrosion Inhibitor Blends for Rebar in Simulated Concrete Pore Solution. *Coatings* **2022**, *12*, 861.

[28]. Zhao, J.; Xu, Y.; Liu, S.; Ding, X. The effect of oxygen-containing species on corrosion behavior of Ta (110) surface: A DFT study with an experimental verification. *App. Surf. Sci.* **2022**, *586*, 152810.

[29]. Assad, H.; Ganjoo, R.; Sharma, S. A theoretical insight to understand the structures and dynamics of thiazole derivatives. *J. Phys. Conf. Ser.* **2022**, *2267*, 012063.

[30]. Park, S. The effects of the leader–member exchange relationship on rater accountability: A conceptual approach. *Cogent Psychol.* **2017**, *4*, 1400416.

[31]. Shanaghi, A.; Souri, A. R.; Chu, P. K. EIS and noise study of zirconia-alumina- benzotriazole nano-composite coating applied on Al2024 by the sol-gel method. *J. Alloys Compd.* **2020**, *816*, 152662.

[32]. Quadri, T. W.; Olasunkanmi, L. O.; Akpan, E. D.; Alfantazi, A.; Obot, I. B.; Verma, C.; Al-Mohaimeed, A. M.; Ebenso, E. E.; Quraishi, M. A. Chromeno-carbonitriles as corrosion inhibitors for mild steel in acidic solution: electrochemical, surface and computational studies. *RSC Adv.* **2021**, *11*, 2462–2475.

[33]. Salmasifar, A.; Edraki, M.; Alibakhshi, E.; Ramezanzadeh, B.; Bahlakeh, G. Combined electrochemical/surface investigations and computer modeling of the aquatic Artichoke extract molecules corrosion inhibition properties on the mild steel surface immersed in the acidic medium. *J. Mol. Liq.* **2021**, *327*, 114856.

[34]. Khaled, M. A.; Ismail, M. A.; El-Hossiany, A. A.; Fouda, A. E.-A. S. Novel pyrimidine-bichalcophene derivatives as corrosion inhibitors for copper in 1 M nitric acid solution. *RSC Adv.* **2021**, *11*, 25314–25333.

[35]. Fouda, A. E.-A. S.; Etaiw, S. E. H.; Hassan, G. S. Chemical, electrochemical and surface studies of new metal-organic frameworks (MOF) as corrosion inhibitors for carbon steel in sulfuric acid environment. *Sci. Rep.* **2021**, *11*, 20179.

[36]. Ansari, K. R.; Quraishi, M. A.; Singh, A. Pyridine derivatives as corrosion inhibitors for N80 steel in 15% HCl: Electrochemical, surface and quantum chemical studies. *Measurement (Lond.)* **2015**, *76*, 136–147.

[37]. Saady, A.; Ech-chihbi, E.; El-Hajjaji, F.; Benhiba, F.; Zarrouk, A.; Rodi, Y. K.; Taleb, M.; El Biache, A.; Rais, Z. Molecular dynamics, DFT and electrochemical to study the interfacial adsorption behavior of new imidazo[4,5-b] pyridine derivative as corrosion inhibitor in acid medium. *J. Appl. Electrochem.* **2021**, *51*, 245–265.

[38]. Saady, A.; Rais, Z.; Benhiba, F.; Salim, R.; Ismaily Alaoui, K.; Arrousse, N.; Elhajjaji, F.; Taleb, M.; Jarmoni, K.; Kandri Rodi, Y.; Warad, I.; Zarrouk, A. Chemical, electrochemical, quantum, and surface analysis evaluation on the inhibition performance of novel imidazo[4,5-b] pyridine derivatives against mild steel corrosion. *Corros. Sci.* **2021**, *189*, 109621.

[39]. Tang, J.; Hu, Y.; Han, Z.; Wang, H.; Zhu, Y.; Wang, Y.; Nie, Z.; Wang, Y. Experimental and theoretical study on the synergistic inhibition effect of pyridine derivatives and sulfur-containing compounds on the corrosion of carbon steel in CO₂-saturated 3.5 wt.% NaCl solution. *Molecules* **2018**, *23*, 3270.

[40]. Thakur, A.; Kumar, A. Sustainable inhibitors for corrosion mitigation in aggressive corrosive media: A comprehensive study. *J. Bio- Tribo-Corros.* **2021**, *7*, 67.

[41]. Thakur, A.; Kaya, S.; Abousalem, A. S.; Sharma, S.; Ganjoo, R.; Assad, H.; Kumar, A. Computational and experimental studies on the corrosion inhibition performance of an aerial extract of Cnicus Benedictus weed on the acidic corrosion of mild steel. *Process Saf. Environ. Prot.* **2022**, *161*, 801–818.

[42]. Parveen, G.; Bashir, S.; Thakur, A.; Saha, S. K.; Banerjee, P.; Kumar, A. Experimental and computational studies of imidazolium based ionic liquid 1-methyl- 3-propylimidazolium iodide on mild steel corrosion in acidic solution. *Mater. Res. Express* **2020**, *7*, 016510.

[43]. Thakur, A.; Kaya, S.; Kumar, A. Recent trends in the characterization and application progress of nano-modified coatings in corrosion mitigation of metals and alloys. *Appl. Sci. (Basel)* **2023**, *13*, 730.

[44]. Bashir, S.; Lgaz, H.; Chung, I.-M.; Kumar, A. Effective green corrosion inhibition of aluminium using analgin in acidic medium: an experimental and theoretical study. *Chem. Eng. Commun.* **2021**, *208*, 1121–1130.

[45]. Thakur, A.; Kumar, A. A review on thiazole derivatives as corrosion inhibitors for metals and their alloys. *Eur. J. Mol. Clin. Med.* **2020**, *7*, 3702–3712.

[46]. Thakur, A.; Kaya, S.; Kumar, A. Recent innovations in nano container-based self-healing coatings in the construction industry. *Curr. Nanosci.* **2022**, *18*, 203–216.

[47]. Chen, L.; Lu, D.; Zhang, Y. Organic compounds as corrosion inhibitors for carbon steel in HCl solution: A comprehensive review. *Materials (Basel)* **2022**, *15*, 2023.

[48]. Kang, Q.; Wang, G.; Liu, Y.; Chen, Y.; Luo, S. Experimental and theoretical study for hot corrosion behavior of network structured TiBw/TA15 composite with NaCl film at 800℃. *Corrosion Science* **2022**, *206*, 110540.

[49]. Arafa, W. A. G. A.; El-Sayed, N. H. Synthesis and corrosion inhibition evaluation of novel aminic nitrogen-bearing 1,2,4-triazole Schiff base compounds. *Eur. J. Chem.* **2014**, *5*, 563–569.

[50]. Bourzi, H.; Oukhrib, R.; El Ibrahimi, B.; Abou Oualid, H.; Abdellaoui, Y.; Balkard, B.; El Issami, S.; Hilali, M.; Bazzi, L.; Len, C. Furfural analogs as sustainable corrosion inhibitors—predictive efficiency using DFT and Monte Carlo simulations on the Cu(111), Fe(110), Al(111) and Sn(111) surfaces in acid media. *Sustainability* **2020**, *12*, 3304.

[51]. Motawea, M. S.; Abdelaziz, M. A. Some pyrazole derivatives as corrosion inhibitors for carbon steel in hydrochloric acid solutions. *Eur. J. Chem.* **2015**, *6*, 342–349.

[52]. Benarioua, M.; Mihi, A.; Bouzeghaia, N.; Naoun, M. Mild steel corrosion inhibition by Parsley (Petroselium Sativum) extract in acidic media. *Egypt. J. Pet.* **2019**, *28*, 155–159.

[53]. Begum, A. A. S.; Vahith, R. M. A.; Kotra, V.; Shaik, M. R.; Abdelgawad, A.; Awwad, E. M.; Khan, M. Spilanthes acmella leaves extract for corrosion inhibition in acid medium. *Coatings* **2021**, *11*, 106.

[54]. Hossam, K.; Bouhlal, F.; Hermouche, L.; Merimi, I.; Labjar, H.; Chaouiki, A.; Labjar, N.; Malika, S.-I.; Dahrouch, A.; Chellouli, M.; Hammouti, B.; El Hajjaji, S. Understanding corrosion inhibition of C38 steel in HCl media by omeprazole: Insights for experimental and computational studies. *J. Fail. Anal. Prev.* **2021**, *21*, 213–227.

[55]. Berisha, A. Experimental, Monte Carlo and Molecular Dynamic study on corrosion inhibition of mild steel by pyridine derivatives in aqueous perchloric acid. *Electrochem* **2020**, *1*, 188–199.

[56]. Verma, C.; Rhee, K. Y.; Quraishi, M. A.; Ebenso, E. E. Pyridine based N-heterocyclic compounds as aqueous phase corrosion inhibitors: A review. *J. Taiwan Inst. Chem. Eng.* **2020**, *117*, 265–277.

[57]. Ansari, K. R.; Quraishi, M. A.; Singh, A. Corrosion inhibition of mild steel in hydrochloric acid by some pyridine derivatives: An experimental and quantum chemical study. *J. Ind. Eng. Chem.* **2015**, *25*, 89–98.

[58]. Lashkari, M.; Arshadi, M. R. DFT studies of pyridine corrosion inhibitors in electrical double layer: solvent, substrate, and electric field effects. *Chem. Phys.* **2004**, *299*, 131–137.

[59]. Saxena, A.; Kumar, J. Phytochemical screening, metal-binding studies and applications of floral extract of Sonchus oleraceus as a corrosion inhibitor. *J. Bio- Tribo-Corros.* **2020**, *6*, 55.

[60]. Thomas, A.; Prajila, M.; Shainy, K. M.; Joseph, A. A green approach to corrosion inhibition of mild steel in hydrochloric acid using fruit rind extract of Garcinia indica (Binda). *J. Mol. Liq.* **2020**, *312*, 113369.